
Article:
Sturge, D., Sobotta, D., Howell, R.J. et al. (2015) A hybrid actuator disc - full rotor CFD methodology for modelling the effects of wind turbine wake interactions on performance. Renewable Energy, 80. pp. 525-537. ISSN: 2314-4394

https://doi.org/10.1016/j.renene.2015.02.053

A Hybrid Actuator Disc – Full Rotor CFD Methodology for Modelling the Effects of Wind Turbine Wake Interactions on Performance

D. Sturge[a,b*], D. Sobotta[b], R. Howell[a,b], A. While[a,c], J. Lou[d]

[a]*WindNet, The University of Sheffield, UK*

[b]*Department of Mechanical Engineering, The University of Sheffield, Mappin Street, Sheffield, S1 3JD, UK*

[c]*Department of Town & Regional Planning, The University of Sheffield, Western Bank, Sheffield, S10 2TN, UK*

[d]*Institute of High Performance Computing, Fusionopolis, 1 Fusionopolis Way, #16-16 Connexis, 138632, Singapore*

**Corresponding author at: Department of Mechanical Engineering, The University of Sheffield, Mappin Street, Sheffield S1 3JD, UK. Tel: +44 7515 668058. E-mail address: d.sturge@sheffield.ac.uk (D. Sturge).*

Abstract

The performance of individual wind turbines is crucial for maximum energy yield. However, this is often reduced when individual wind turbines are placed together in an array. The wake produced by the rotors interacts with downstream turbines, resulting in a reduction in power output. In this paper, we demonstrate a new faster modelling method by combining actuator disc theory, modelled using wind tunnel validated Computational Fluid Dynamics (CFD), integrated to full rotor CFD simulations. This novel hybrid of techniques results in the ability to analyse performance when simulating various array layouts more rapidly and accurately than using either method on its own.

It is shown that there is a significant power reduction from a downstream turbine that is subjected to the wake of an upstream turbine, and that this is due to both a reduction in power in the wind and also due to changes in the aerodynamics of the

downstream turbine itself. Analysis of static pressure along the blade showed that as a result of wake interactions, a large reduction in the suction peak along the leading edge reduced the lift generated by the rotor and so reduced the torque production and the ability for the blade to extract energy from the wind.

Keywords

Wind turbine wake interactions; wind turbine array performance; computational fluid dynamics; actuator disc; wind tunnel test; hybrid simulation technique

Introduction

Increased pressure to maximise the emissions savings and investment returns has led to growing interest in optimising energy yield from wind turbines [1]. One issue is that it can be difficult to anticipate the cumulative impact of multiple wind turbines on each other in a wind farm. Understanding the flow physics and interactions between the wake from one turbine and surrounding wind turbines is crucial to achieving the optimal layout of a wind farm. This issue is examined in the following paper.

Wind energy developments are a contentious issue within the UK planning system. Unlike countries such as Germany and Denmark, where wind farms are generally accepted as a reliable source of renewable energy [2], [3], in the UK the matter of energy yield is lower on the list of priorities, especially compared with potential visual and noise impacts [1]. Despite the National Planning Policy Framework [4] that explicitly supports the developments of low-carbon projects in order to reduce the effects of climate change; there is often a significant compromise in optimal wind turbine layouts in a farm situation as a result of the need to site turbines in locations that allow for visual amenity rather than maximising power output. The problem stems from a lack of understanding and ability for developers to communicate the effects that wind farm layouts have on performance, and therefore, viability. The inherent negative view that wind energy has is partly a result of poorly laid out wind farms due to issue described above, and this downward spiral continues. The methodology developed in this paper aims to improve the fundamental knowledge of wind turbine performance when placement is less than optimal, and allow for quantified results that can be used to bolster wind energy developments.

Wind Turbine Wake

Research into the area of HAWT aerodynamics and maximising efficiency began in 1920 with the publication of the Betz limit [5]. This set a precedent for the field of wind turbine aerodynamics with the discovery that, theoretically, no more than 59.3% of the kinetic energy of a fluid contained in a stream tube with the same cross sectional area as a rotor disc may be converted into useful work. Since then the aerodynamics of wind turbines have been studied, Vermeer et al. suggests that the efficiency has improved

from 40% to 50% [6]. However, much of the flow physics is still not fully understood; for example the interactions of wake between wind turbines.

In a wind farm made up of multiple rows, the downstream wind turbine sees the combined effects of the incoming flow and the disturbance caused by the upstream turbines. This latter flow i.e. the wake, is a region of low velocity fluid coupled with high turbulence. As a result, a wind turbine sitting in the wake of another potentially has a greatly reduced energy yield due to a diminished wind speed [7]. The wake itself is generally divided into two separate regions known as the near and far wake regions [6]. The near wake region is found within the distance of three rotor diameters (3D) downstream of the wind turbine; in this region, the properties of the turbine (number of blades and blade aerodynamics) are of importance. Beyond this region is known as the far wake; where the finer details of the flow have been mixed out, but the velocity deficit still remains. These two regions are of course related because the characteristics of the far wake are dependent on the near wake and the wind turbine. However, the focus of this paper will be on the far wake region as it is this area that determines the aerodynamics of a wind farm.

Actuator Disc Theory

The actuator disc (AD) technique is often used for simulating wakes in wind farms, because of the model's ability to reliably replicate the far wake region and interactions with other wakes [8]. In the context of this paper, ADs are simply used as a tool for generating appropriate wake velocity deficits. The concept can be applied to both experimental and numerical modelling techniques. The flow field behind the wind turbine rotor is simulated using a simplified technique that lets the user to mimic the energy extraction from a wind turbine without having to model specific rotor geometry [9]. The axial induction factor, a, allows mean velocity of the wake to be quantified (Equation (1)):

$$U_{wake} = (1 - 2a)U_{\infty} \quad (1)$$

Where U_{∞} is the mean upstream velocity at height of the turbine hub.

For experiments, wire meshes can be used (amongst other methods) with different porosities to create different wake characteristics. The porosity is the

97 percentage of void space (open area) of the total surface area over a porous disc;
98 altering this allows the user to determine, by choice of induction factor, what the wake
99 of the modelled wind turbine will behave like.

100 The following sections describe the experimental and numerical methods applied in
101 this study; with the wind tunnel experiments acting as a form of validation for the
102 Computational Fluid Dynamics (CFD) simulations. This is followed by further CFD
103 simulations of a full rotor that is applied with a new technique to measure the
104 performance within a wind turbine array.

105 # 1 Validation

106 Simulating wake interactions on multiple full rotors in a single computational
107 domain is not impossible as shown by Weihing et al. [10], however, due to limitations of
108 available computational power means it is currently unrealistic to perform such
109 simulations within the development cycle of a wind farm and when modelling multiple
110 layouts. This is because of the increased mesh density required downstream of the rotor
111 to accurately capture of flow physics of the far wake. Therefore, a new technique of
112 extracting the data collected from the actuator disc method and applying it upstream of
113 a high fidelity wind turbine CFD has been developed. The advantage of the new method
114 is that the computational cost and time is kept low, while still having the ability to
115 analyse detailed full rotor performance in various array layouts.

116 For the purposes of this paper, the actuator disc method will be used to replicate
117 the far wake region of a wind turbine. Current CFD packages allow for porous mediums
118 to be simulated, however, there is a requirement for this to be validated with the use of
119 experimental work carried out in wind tunnel. This section describes the process of
120 validation carried out.

121 ## 1.1 Experimental - Wind Tunnel Facility

122 The Department of Mechanical Engineering at The University of Sheffield has a
123 low-speed wind tunnel (Figure 1.1) which has been used for the experimental work in
124 this paper.

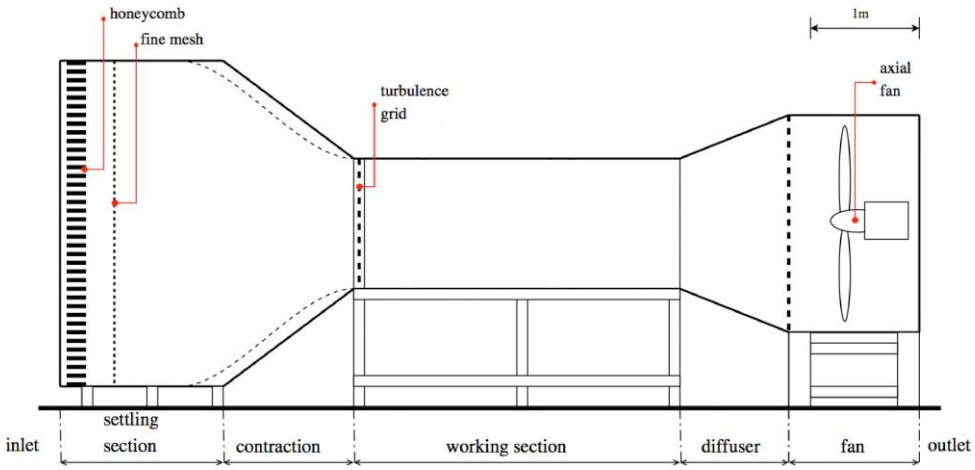

Figure 1.1 Wind tunnel schematic (not to scale).

The wind tunnel is an open circuit suction tunnel, driven by an eight-blade axial fan positioned at the outlet. The flow enters the inlet, going through a honeycomb mesh (with cells 0.01 m wide and 0.1 m long) that straightens the flow and breaks any large-scale flow structures. The flow then streams through a fine 1 mm cell mesh screen to further break down flow structures as well as evening out the flow with the generation of small scale turbulence and a pressure drop. The flow settles before being accelerated by a 6.25:1 contraction section leading to a turbulence grid at the entrance of the 1.2 m high x 1.2 m wide x 3 m long test section. The fan itself is controlled using a variable frequency drive that allows for precise control of the wind speed, with a maximum of 25 ms^{-1}.

1.1.1 Experimental Design

The aim of the experiments was to measure the wake behind a porous disc at a range of distances downstream. A 100 mm in diameter metal mesh disc was used to replicate the rotor of a wind turbine; the disc has an open area of 45%, with a wire diameter of 280 μm and a nominal gap aperture of 0.567 mm, which resulted in a measured induction factor of 0.34. Figure 1.3 shows the mesh disc attached to a rod 400 mm above a removable floor in the wind tunnel that allows the disc to be placed in various positions of 200 mm apart, or 2D. This allowed for wake measurements

downstream at 2D, 4D, 6D, 8D and 10D, which were taken at velocities 10 ms^{-1}, 7.5 ms^{-1} and 5 ms^{-1}.

Using a reference length of 0.1 m (the diameter of the actuator disc), the Reynolds number at 10ms^{-1} is 6.2x10^4, which is two orders of magnitude lower than that experienced by full size wind turbines. However, the Reynolds number becomes less important when modelling the far wake using an actuator disc [11]. Whale et al. [12] also showed that the characteristics of the wake are mostly independent of the blade Reynolds number. Therefore, validating the AD method in a wind tunnel using a scaled model will not affect the overall correctness of the results.

The velocity measurements were taken using a pitot-static probe, where the pressure difference was measured using a Furness Controls Micromanometer (model FC0510), providing a velocity accuracy of +/-0.5%. The probe was attached to a traverse system (Figure 1.3) and readings were taken horizontally along the centre line at 10 mm intervals behind the disc and at 20 mm apart either side. In order to match the turbulence intensity (T_u) decay in the wind tunnel to the later CFD simulations, measurements were taken using a constant temperature hot-wire anemometer in increments of 0.2 m upstream of the metal disc. It was observed (Figure 1.2) that at the point of the actuator disc, T_u = 1.04%.

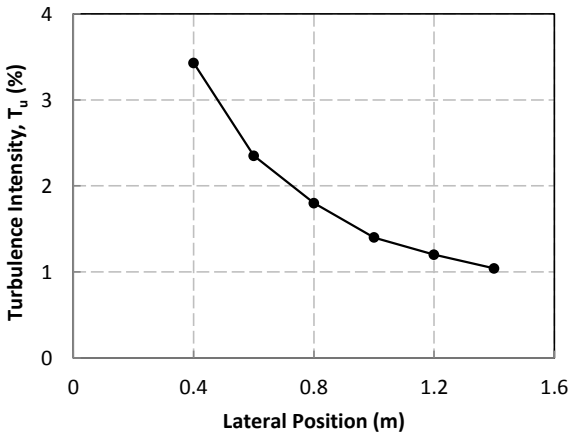

Figure 1.2 Turbulence intensity decay in the wind tunnel (x=0: test section inlet), from [13].

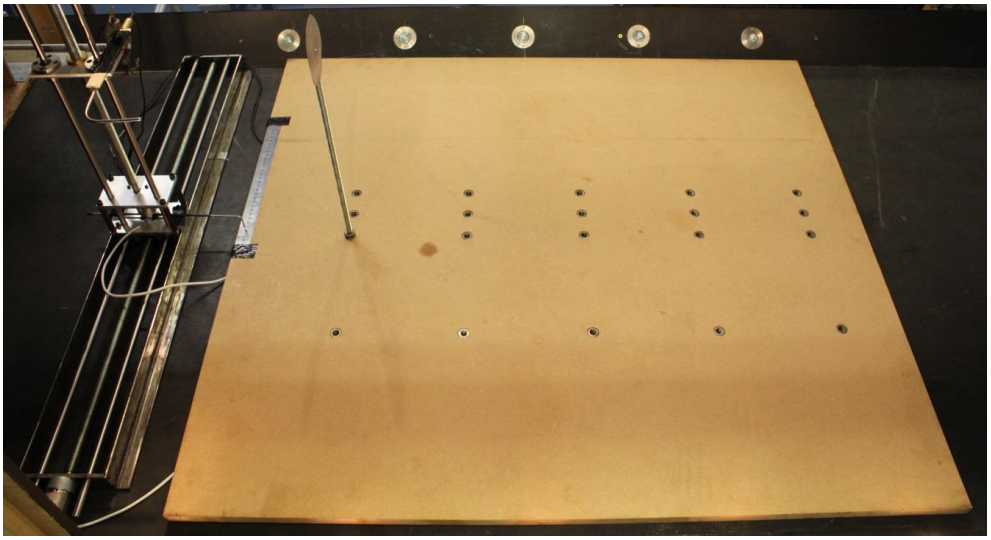

Figure 1.3 Photograph showing the locations available for the porous disc to be positioned within the wind tunnel test section.

1.2 Numerical – Actuator Disc Model

The use of CFD has become a crucial tool in predicting wind turbine wake and interactions. It allows for multiple layouts and conditions to be simulated with relative ease of use, especially in comparison with experimental techniques.

1.2.1 Wind Tunnel Computational Domain

A computational domain that represents the wind tunnel test section discussed in section 1.1 was built using ICEM CFD, Ansys Inc., which gave a minimum domain (containing a single AD as shown in Figure 1.4) that consists of approximately 237,000 Hexa elements. This was achieved via a mesh independence study as described in the next section. All simulations were carried out using the CFD package Ansys Fluent.

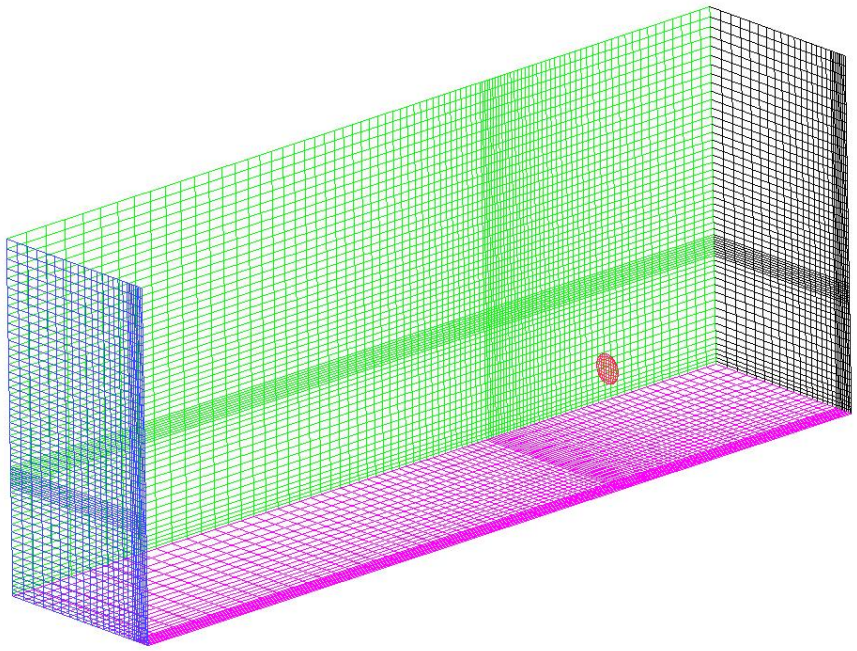

Figure 1.4 Computational mesh visualising half the mesh topology (but the full actuator disc) for the wind tunnel domain.

1.2.2 Boundary Conditions

The boundary conditions (Table 1.1) have been applied so that they replicate the flow field characteristics of the wind tunnel. A steady, coupled solver (for highest accuracy) was selected and all discretisation terms set to 2nd order. In order to define the actuator disc, Ansys Fluent recommends boundary conditions based on experimental data [14]. Experimental data from the wind tunnel in the form of pressure drop against velocity through a porous disc (actuator disc) was extrapolated to determine the coefficients of the medium. In order to replicate the mesh disc qualities used in the wind tunnel for CFD purposes, the following process was applied. A *xy* curve is plotted to create a trendline through these points yielding the following:

$$\Delta p = x^2 - x \tag{2}$$

Using a simplified version of the momentum equation, relating the pressure drop to the source term can be expressed as:

$$\nabla \mathrm{p} = S_i \quad (3)$$

or

$$\Delta p = -S_i \Delta n \quad (4)$$

Hence, comparing Equation (3) to Equation (2) yields the following curve coefficients:

$$x^2 = C_2 \frac{1}{2} \rho \Delta n \quad (5)$$

Where ρ is the density of air, Δn is the porous medium thickness, and C_2 is the inertial resistance factor, which in Fluent is called the Pressure Jump Coefficient. The Face Permeability, α, which is calculated using the viscous inertial resistance factor, $\frac{1}{\alpha}$:

$$-x = \frac{\mu}{\alpha} \Delta n \quad (6)$$

Table 1.1 Boundary conditions used for CFD simulations of the wind tunnel.

Boundary Type	**Specific Condition**	
Velocity Inlet	Velocity Magnitude	10 ms^{-1}
	Turbulent Intensity	8%
	Turbulent Viscosity Ratio	14
Pressure Outlet		
Floor (Wall)	Roughness Height	0.0015 m
Top, Sides (Wall)		
AD (Porous Jump)	Face Permeability (α)	2.57 x 10^{-8} m^2
(Represents an induction factor of 0.34)	Porous Medium Thickness (Δn)	0.0025 m
	Pressure-Jump Coefficient (C2)	807.03

1.2.3 Mesh Independence Study

The number of elements used in a mesh of this kind of domain must be optimised before running a full simulation; this minimises the computational power and time required for the generation of a grid independent solution. Three independent studies were carried out which looked at the optimal number of cells in the axial direction (x-direction), lateral direction (z-direction), and across the AD (y and z-directions). The number of cells in the y-direction above and below the AD has been prescribed based on recommendation for surface boundary layer modelling [15], which yielded 19 cells below and 30 cells above the disc.

In the x-direction the AD itself is only 2.5 mm thick (2.5% of a turbine diameter), therefore, the thickness in terms of mesh remains constant for all cases at two cells. The actual required thickness of the AD is applied within the boundary conditions of Fluent. Table 1.2 shows the test matrix of all the simulations carried out in the mesh independence studies.

Table 1.2 The test matrix for the mesh independence simulations carried out for the wind tunnel domain.

	Number of Cells						
Test Number	**x-direction**			**y-direction**	**z-direction**		
	Upstream	**Disc**	**Downstream**	**Disc**	**Left**	**Disc**	**Right**
Axial Direction							
1	30	1	30	7	18	7	18
2	45	1	45	7	18	7	18
3	60	1	60	7	18	7	18
Lateral Direction							
1	45	1	45	7	12	7	12
2	45	1	45	7	18	7	18
3	45	1	45	7	24	7	24
4	45	1	45	7	30	7	30
Across Disc							
1	45	1	45	5	18	5	18
2	45	1	45	10	18	10	18
3	45	1	45	12	18	12	18
4	45	1	45	12	18	14	18

The results of the mesh independence studies are shown in Figure 1.5; this yielded an optimal mesh that consists of 23 cells/m upstream of the first AD, 45 cells/ downstream each AD thereafter, 18 cells either side of the AD, and 10 cells across the AD itself.

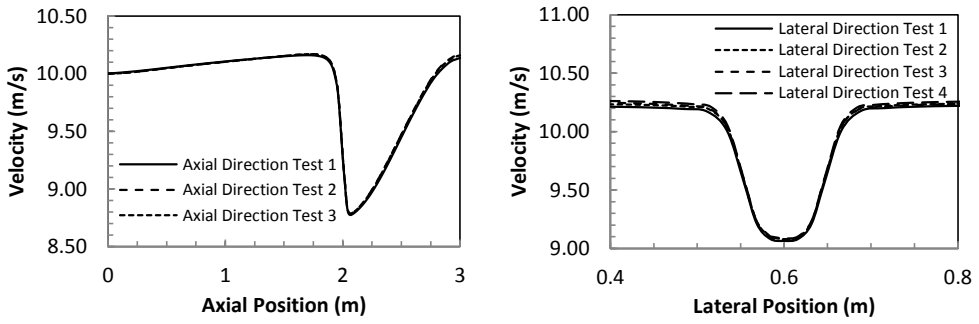

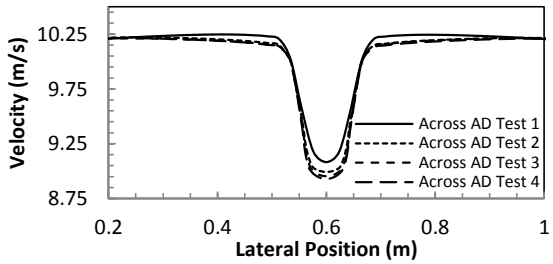

Figure 1.5 Mesh independence studies for the wind tunnel domain in the: axial direction (top left), lateral direction (top right), and number of cells across the actuator disc (bottom middle).

1.2.4 Turbulence Modelling

The velocity in the wind tunnel experiments was set no higher than 10ms^{-1}; this leads to the use of the incompressible Navier-Stokes equations for the CFD simulations. The inlet conditions (Table 1.1) were pre-determined to produce a matching turbulence intensity at the location of the AD observed in the experiment, as shown in Figure 1.6. The decay of the turbulence upstream is not very well matched but at streamwise positions around 1m downstream of the inlet the turbulence matches very well and from a distance of 1.2m is, for the purposes in this paper, the same between the experiment and the CFD.

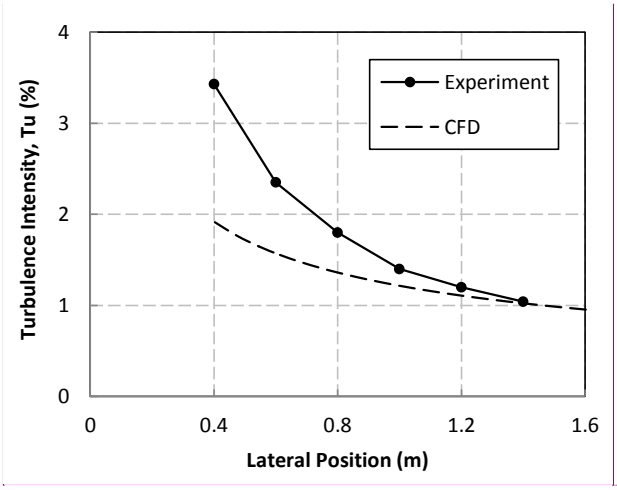

Figure 1.6 Comparison of turbulent intensity between CFD and wind tunnel experiment (x=0: test section inlet).

Comment [R1]: Just realised we essentially have this twice – can we remove one of them and refer back to it as needed?

To appropriately select a turbulence model to replicate the wake from a porous disc, a study was conducted for initial validation. Two-equation turbulence models such as *k-ε* and *k-ω* are widely used for actuator disc CFD simulations due to their ease on computational power and relatively stability in reaching convergence [16]. Both have their advantages, for example the *k-ω* is more accurate in formulating near-wall regions, whereas *k-ε* has free-stream independence in the fair field [17]. In Figure 1.7 and Figure 1.8 the experimental measurements taken from the wind tunnel are compared to the results at the same points from the CFD simulations using three different turbulence models. It is evident at 6D *k-ω* more accurately replicates the wake at this distance, however, further downstream at 10D *k-ε* proves superior.

The *SST k-ω* turbulence model applies the *k-ω* solutions to the inner part of the boundary layer, so it can be used for low Reynolds numbers applications. It then switches to a *k-ε* model in the free stream, where the *k-ω* has difficulties replicating the flow correctly with inlet turbulence properties [17]. Therefore, it was decided that overall the *SST k-ω* turbulence model is most appropriate. This model was also chosen for consistency with the full rotor model that is described further on.

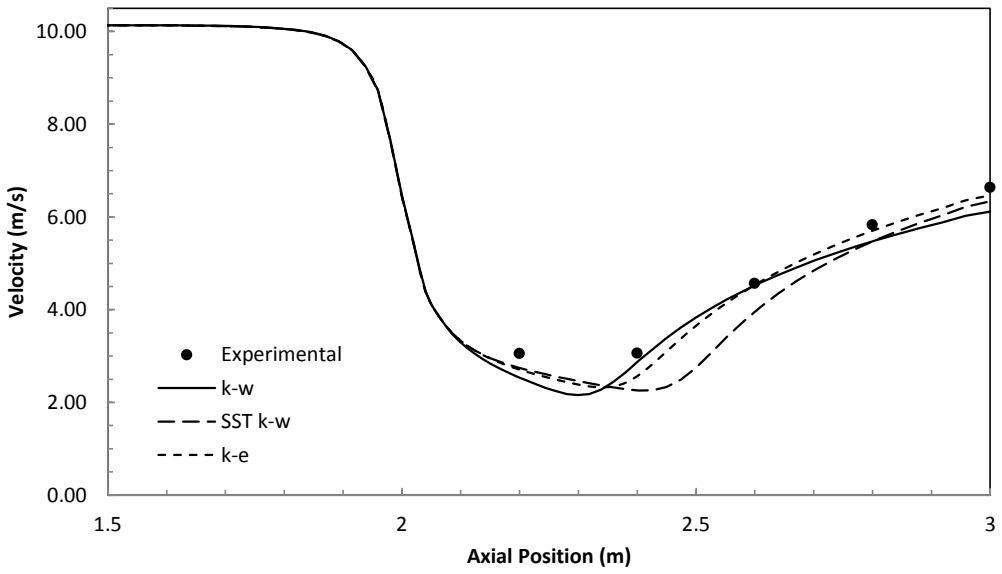

Figure 1.7 Wake recovery predicted by three turbulence models and compared with the wind tunnel experiment results, with an inlet speed of 10 ms^{-1}.

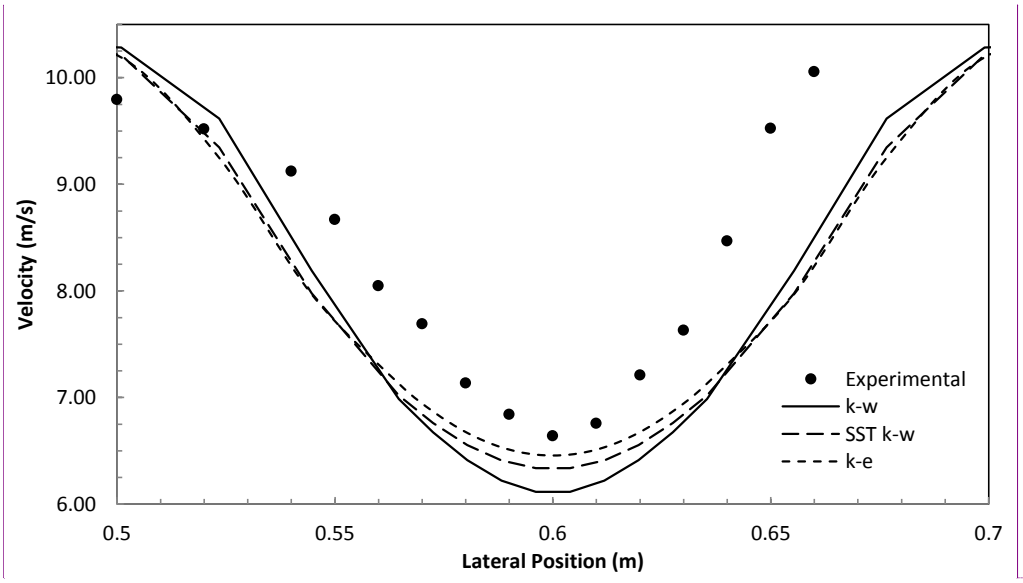

Comment [R2]: Need to make all these graphs (so 1.7 as well) non-dimensional if we've done so for 1.9.

Figure 1.8 Wake velocity profiles predicted by three turbulence models at 10D downstream of the porous disc.

1.2.5 Numerical vs. Experimental Results

For the purpose of this research, the experiments carried out in the wind tunnel are used to validate the CFD technique, which has been done by comparing both sets of data (Figure 1.9). Work carried out by Cabezon et al. [18] compared different turbulence models against experimental data to show the ability for the actuator disc to replicate the far wake of a wind turbine. It was shown that while the ability for the wake to recover, overall shape of the wake and maximum velocity deficit was simulated correctly; the wake width did not match up. This is also the case for the research carried out in this paper. There is also a marginal difference in centreline velocities, however, in the far wake this becomes minimal and this is the area of interest when applying the actuator disc method. Overall this shows that the actuator disc technique and current turbulence modelling is not a perfect way to represent the far wake by any means, but it is more than acceptable for the purposes of this paper.

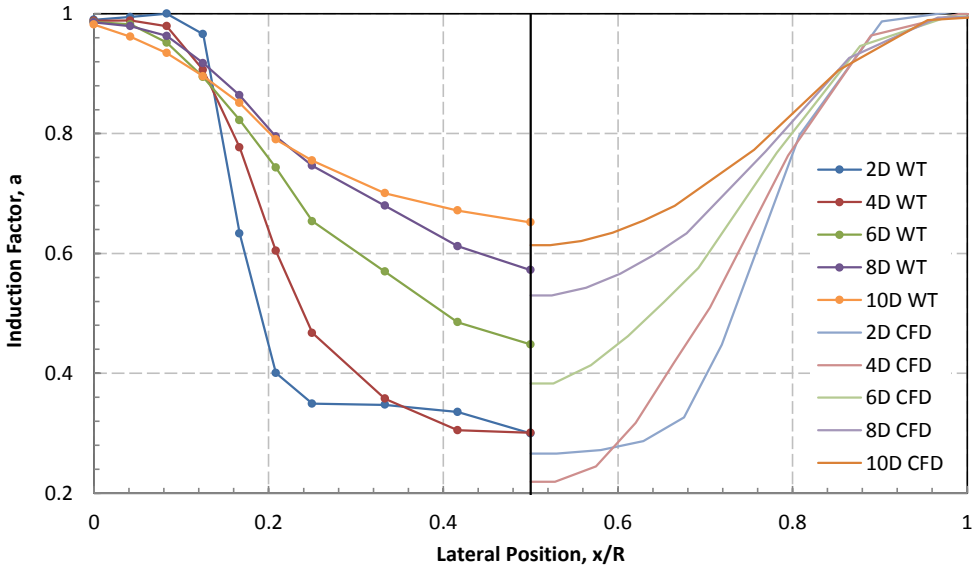

Figure 1.9 Comparing numerical and experimental results with an inlet speed of 10ms^{-1}.

This technique has been adequately validated by wind tunnel experiments and is suitable for predicting the physics of wake development required for this paper. Using this information, it is now possible to tailor and replicate the far wake of a wind turbine with confidence by adjusting the induction factor of a porous disc.

2 Hybrid Actuator Disc – Full Rotor Method

The development of this technique combines the validated actuator disc method within CFD and a full high fidelity CFD wind turbine rotor model.

A full rotor CFD model was created replicating the two bladed NREL Phase VI rotor, using the software Gridgen and TGrid. The full computational domain extended 2, 3 and 2.5 diameters in the upstream, downstream and radial direction. The flow enters the computational domain through a velocity inlet, passes the turbine blades that were modelled using a no-slip wall and the flow exits via a pressure outlet boundary. The cylindrical outer edge was modelled using the symmetry boundary condition.

Figure 2.1 shows the topology of an 180° section the full rotor mesh; the mesh of the second blade is identical to that shown. The reason for using a 2-bladed full 360° mesh is to allow for non-symmetrical layouts to be simulated. While the far-field block

(Block 4) is fully structured, the inner domain is made of a hybrid mesh to allow heavy clustering of the cells around the blades to fully resolve the complex flow. Both blades are surrounded by a structured boundary layer (Block 1) which is enclosed by an unstructured block (Block 2) to allow the mesh to transition to a comparable mesh density of that of the far-field block. The unstructured block then connects to a structured domain (block 3) which has minimum thickness of 4 cells before reaching the interface between the stationary and rotating blocks to reduce numerical inaccuracies associated with unstructured meshes.

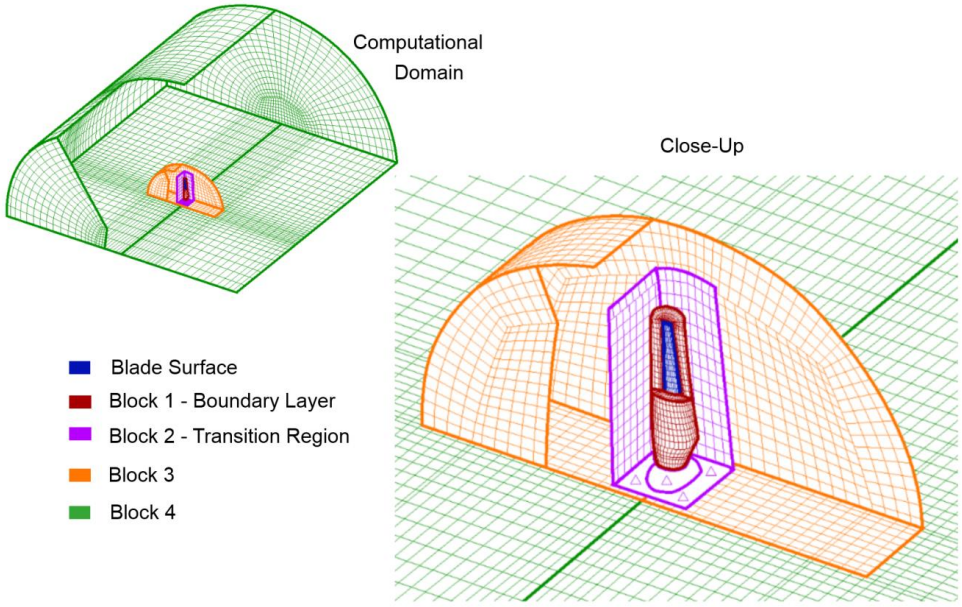

Figure 2.1 Computational mesh visualising mesh topology

An extensive mesh independence study has been conducted using the described mesh topology and validated against experimental data from the project carried out in the NASA Ames wind tunnel [19]. The total grid sizes of the meshes analysed ranged from 8.4×10^6 to 25.2×10^6 cells as described in Table 2.1, which also contains detailed information about the corresponding number of nodes in the boundary layer of each grid. For all the mesh densities the far field (Block 4) remained constant at 6 million cells.

Table 2.1 Cell count of meshes of varying density and detailed boundary layer grid description.

Mesh Density	Cells (x10^6) Total (Including Block 4)	Boundary Layer (Block 1)	Transition (Block 2 and 3)	Nodes Span Wise	Nodes Chord Wise	Growth Rate
Very Coarse	8.4	1.2	1.2	84	116	1.1 increasing to 1.2
Coarse	10.4	2.6	1.8	115	176	1.1 increasing to 1.2
Medium	12.4	5.2	3.2	161	248	1.1 increasing to 1.2
Fine	25.2	13.8	5.4	227	360	1.1

Figure 2.2 shows the results of the mesh independence study. In the validated test case the wind speed was 10 ms^{-1} and turbine rotated at 72 rpm, which resulted in a tip-speed ratio (λ) of 5.4. It can be seen that results of all meshes are in close agreement. For this reason the mesh labelled 'Coarse Mesh' has been chosen for further studies; around the blades there is a Y$^+$ of approximately 0.8 for the operating conditions tested and is therefore suitable for the use with the *SST k-ω* turbulence model.

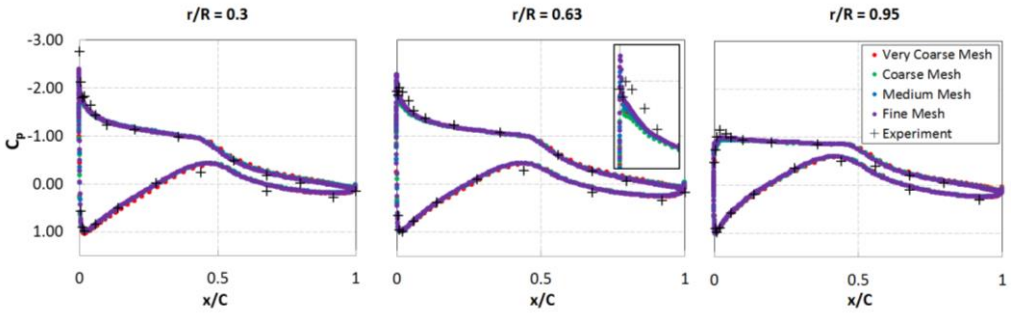

Figure 2.2 Mesh independence/validation results at TSR=5.4.

2.1 Combing Actuator Disc and Full Rotor Models

Combing the two techniques allows for a novel way of analysing performance of a wind turbine in the wake of another. In order to achieve this, an actuator disc simulation of the same diameter as the NREL rotor was constructed. Once this simulation fully converges, the velocity field (an example is presented in Figure 2.3) at any desired point can be extracted and then applied as the inlet boundary condition

velocity field for the full rotor simulation. The flow chart found in Figure 2.4 describes how the two techniques have been combined.

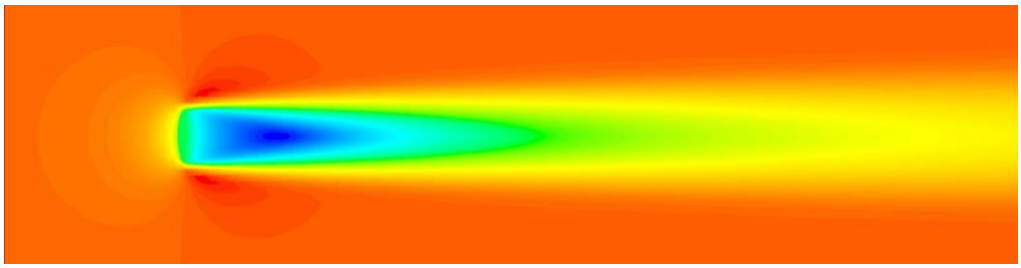

Figure 2.3 Velocity magnitude contour plot of a wind turbine wake using the actuator disc technique (Red = 10 ms^{-1} and Blue = 5 ms^{-1}).

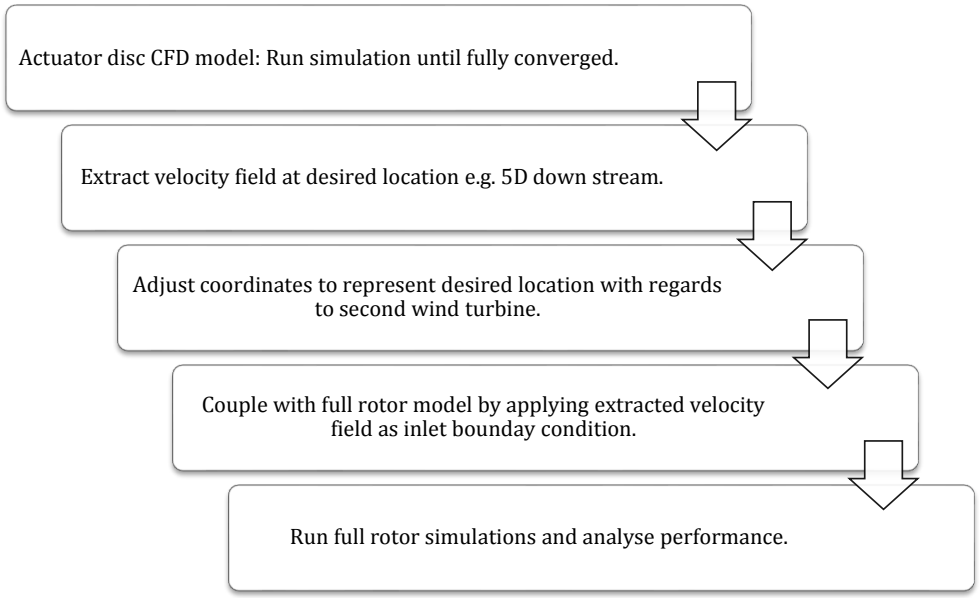

Figure 2.4 Flow chart of the methodology for the hybrid CFD simulations.

Due to the transient nature of the full rotor model and the effect of the offset AD resulting in non-uniform conditions flowing onto the turbine, the simulation was allowed to complete eight full turbine rotations to allow for periodic convergence before any data could be collected. This can be seen in Figure 2.5. This plot shows the torque produced by each turbine blade through the evolution of the solution. It can be seen that periodicity is not reached until the 5th second, which corresponds to the 8th revolution.

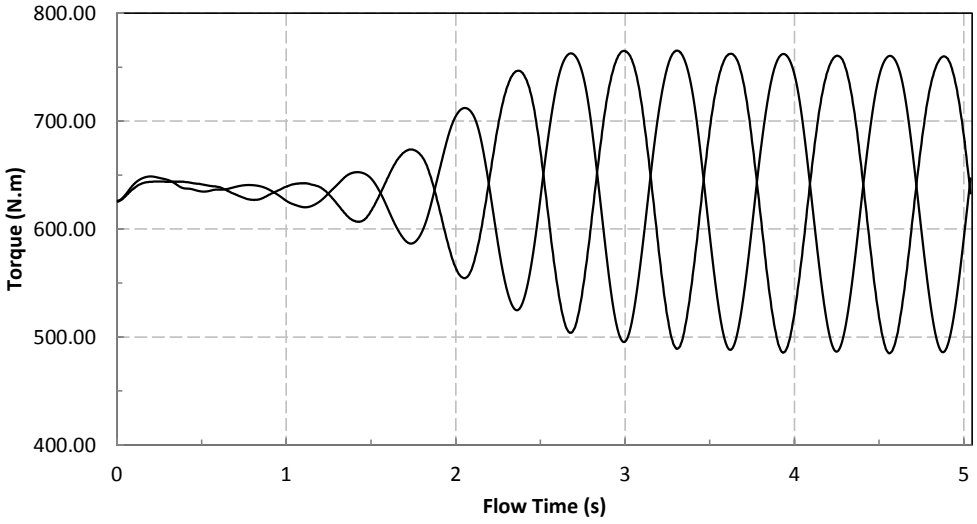

Figure 2.5 The full rotor simulation reaching convergence after eight rotations.

2.2 Reference Cases

For the purposes of the reference cases, thirteen layouts were investigated as illustrated in Figure 2.6. An ideal case was first simulated; for this the full rotor model had a constant inlet velocity of 10 ms^{-1} for which all other cases are compared to. The top set looks at one actuator disc upstream of a full rotor, applying the method described in section 2.1, at distances[1] of 5D, 7D and 10D and for each case the two wind turbines are aligned at their centres and, offset by 0.5D and 1D. The bottom set models three turbines consisting of two actuator discs and a full rotor, each at 7D apart with the same three alignments used in the top set.

[1] One diameter (D) for this case is equal to 10 m.

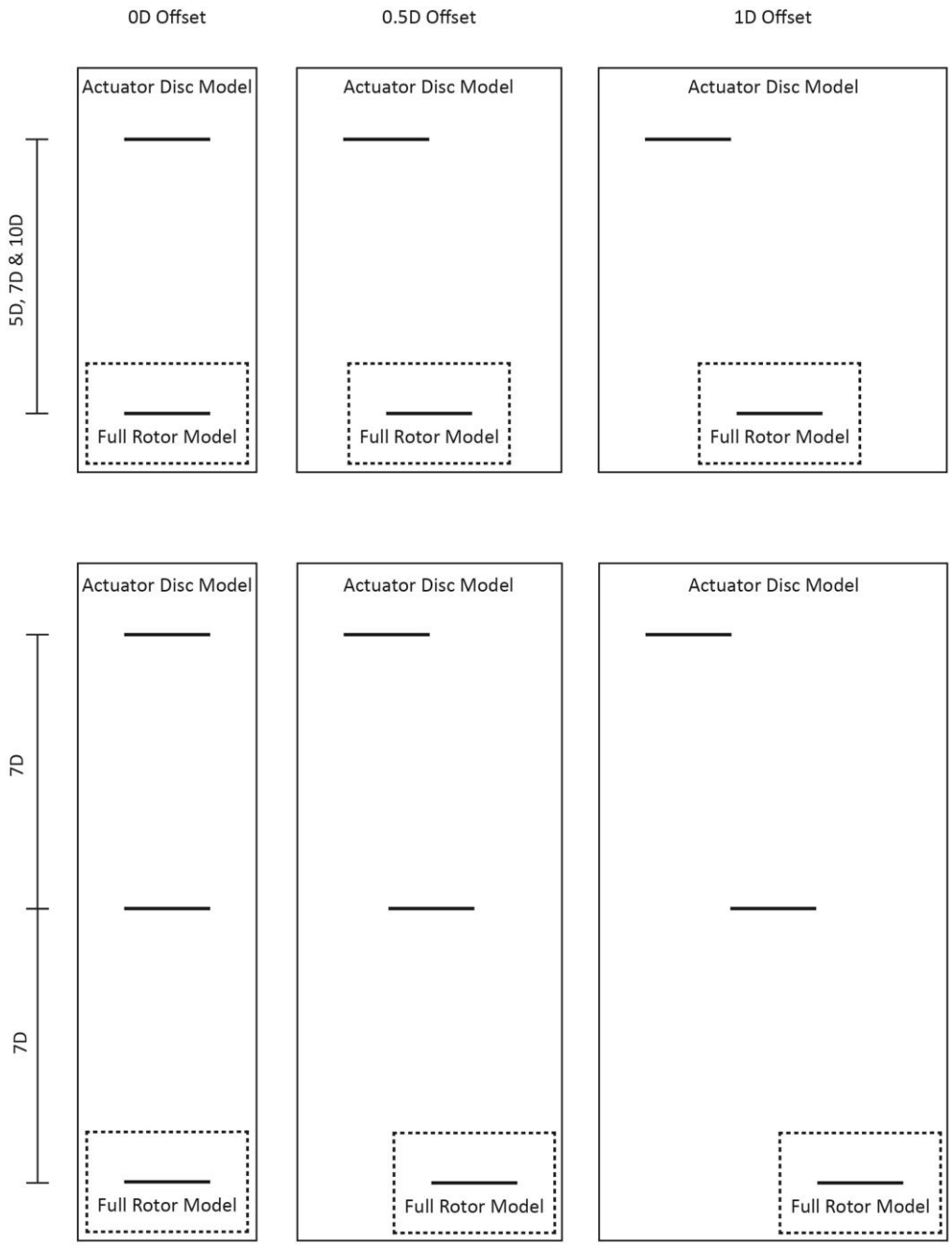

Figure 2.6 The reference cases used to study the effects of wake on wind turbine performance. One actuator disc placed upstream of the full rotor model at distance of 5D, 7D and 10D and offset by 0D, 0.5D and 1D (top). Two actuator discs upstream of the full rotor model at a distance of 7D between each and offset 0D, 0.5D and 1D (bottom). Note: the lines surrounding the cases do not represent the computational domain size used.

3 Results and Discussion

The coefficient of power (CP) provides the simplest, yet most valuable description of a wind turbine's performance; Figure 3.1 shows the CP for the thirteen cases described above. The CP calculated here uses the undisturbed wind speed (i.e. without any upstream turbine present) in the denominator of the definition of power coefficient. However, the power available in the wind to the downstream turbine is reduced due to the presence of the upstream turbine, so it could be argued that the actual power in the wind should be used in the calculation of CP. However, the interest lies in the reduction of power from the downstream turbine, therefore, it is appropriate to use the undisturbed wind speed to calculate the power coefficient.

The CP of each reference case were normalised against the ideal, which had an undisturbed velocity inlet. It can be seen that overall the effect of the upstream turbine results in an interaction that is detrimental to the performance of the downstream turbine. However, the extent to which this occurs varies with layout and distance. As expected, the most severe drop in power is experienced when the two wind turbines are aligned at their centres. An increase in separation distance between the turbines improves the CP of the downstream turbine significantly, with a 44.5% rise with a doubling the distance from 5D to 10D. A similar trend is shown when the two turbines have an offset alignment of half a diameter, but with an overall improved CP. Counterintuitively, when the turbines are misaligned by one diameter and the distances between increases, the CP decreases. An explanation for this occurring is the diverging wake produced by the first wind turbine interacts less at a distance of 5D, but as the distance increases so does the wake width and, therefore, more of the downstream turbine rotor ends up in the wake and this outweighs the recovery in the flow velocity. Figure 3.2 shows the wake recovery behind the actuator disc as viewed from the centreline of the downstream wind turbine for the three layouts simulated. The explanation for an increased CP with a decreasing downstream distance for the 1D offset case is seen with a slight rise in wind speed at the point of the first turbine before a fall to a 'recovered' velocity.

In a three-turbine layout, the performance of the wind turbine of interest differs when compared with two turbines. As shown in research carried out by Stevens et al. [20] and Porté-Agel et al. [21], when the wind turbines are aligned the most effected

turbine is found in the second row, after which there is a slight increase in performance of the following rows. This is the opposite case when wind turbines are offset by half a diameter, because of the diverging wake and the lack of power available from the incoming wind. When offset by one diameter, the diverging wake at this distance from the first turbine is likely to have little effect on third turbine in comparison to the second, explaining the increase in CP at this point.

It is acknowledged that in reality a wind turbine will employ a control system to adjust the TSR of the rotor when in the wake of another to try achiever a higher CP.

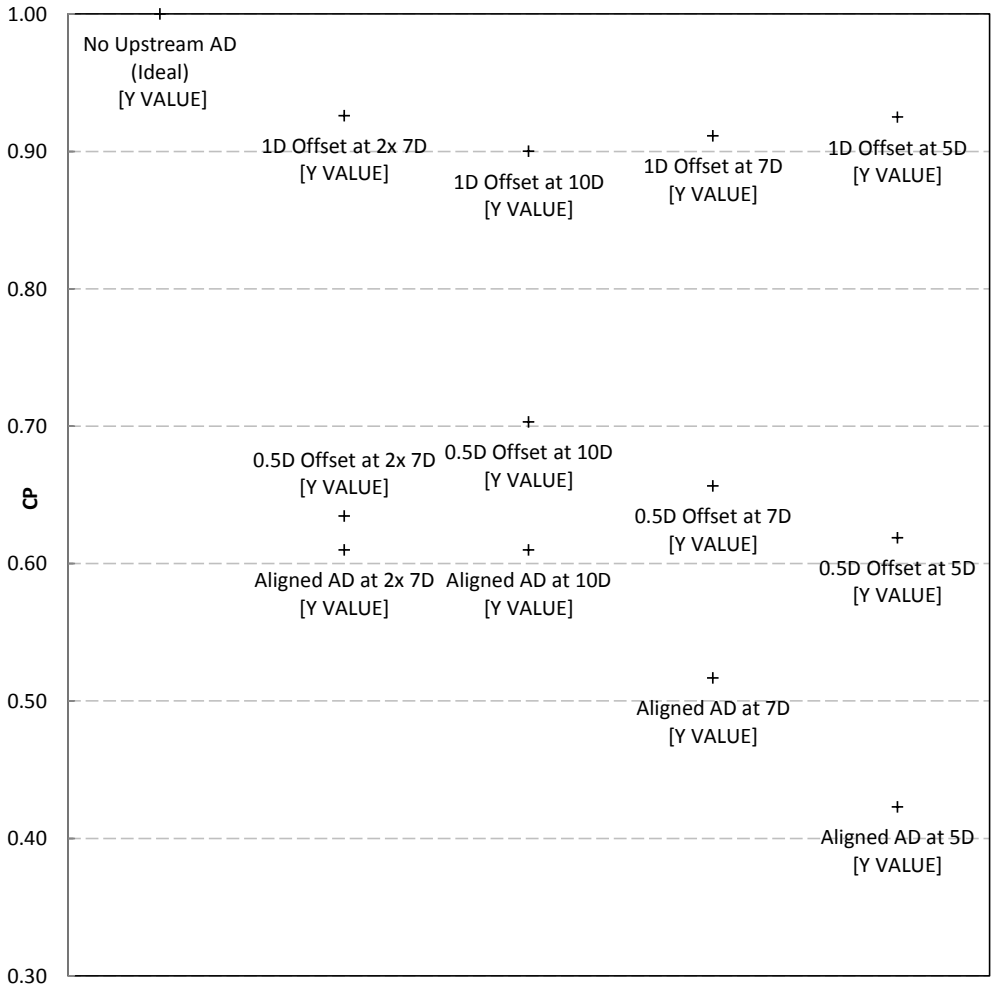

Figure 3.1 Comparing the normalised Coefficient of Power (CP) from all reference cases.

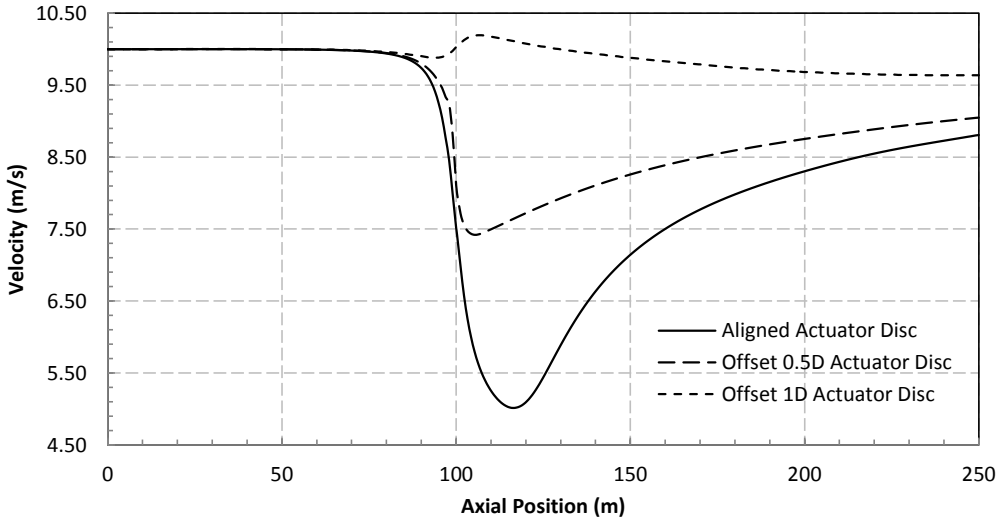

396

397 **Figure 3.2 The wake recovering behind a single actuator disc at the centre lines for the three alignment cases.**

398 Currently, wind farms conventionally use a turbine spacing of approximately 7D
399 [22], for this reason the 7D cases will be discussed in further detail. The plots in Figure
400 3.3 compare the coefficient of pressure (C_p) around one of the blades at three radial
401 locations from root to tip for the range of simulations carried out. Beginning with the
402 comparison of the ideal case and when fully aligned, the reduction in power is evident
403 due a dramatic drop in leading edge suction peak, especially in the lower two-thirds of
404 the blade. This is the result of a lower wind speed experienced, which reduces the life
405 that the blade generates along with a reduced torque and power. The reduced wind
406 velocity also has a direct effect on circulation around the blade, again reducing lift. The
407 leading edge peak in pressure coefficient difference is also shown for the cases of 0.5D
408 and 1D offset, these two graphs compare the same blade when fully inside and outside
409 of the incoming wake. The blade is able to produce a higher amount of lift when outside
410 of the wake, even for the 1D offset case where this difference is only slight, but enough
411 to reduce the overall efficiency of the wind turbine.

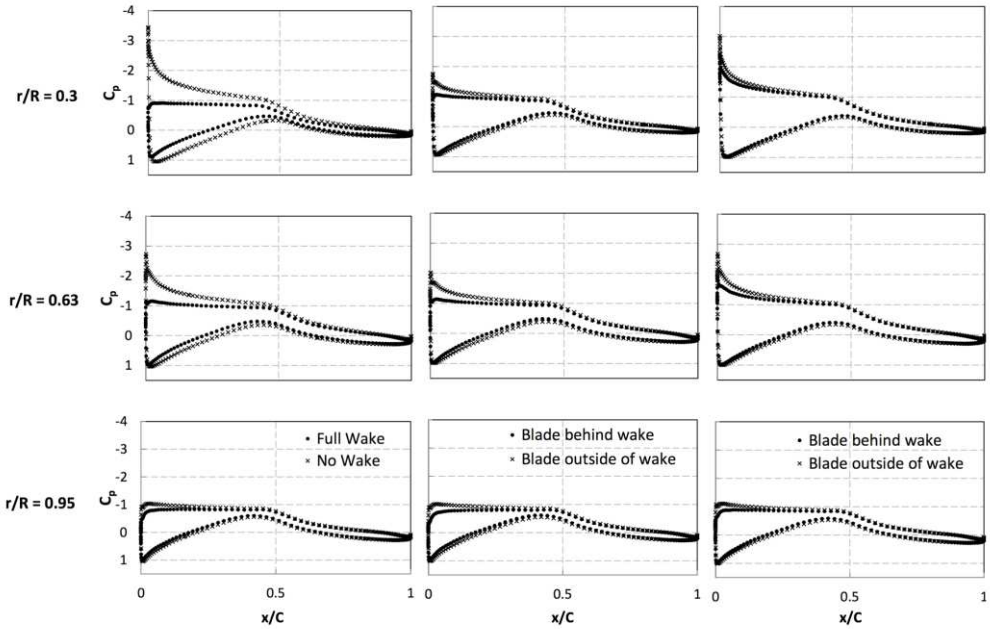

412

413 **Figure 3.3 C_p plots along the blade at three radial distances for 7D cases: AD aligned with rotor versus no**
414 **upstream AD (left), AD offset 0.5D with rotor (middle) and, AD offset 1D with rotor (right).**

415 Pressure contour plots along the blades for the four cases are shown in Figure 3.4;
416 in general it is evident that there is a large reduction in negative pressure coefficient at
417 the leading edge along the length of the blade when in the wake of another wind
418 turbine. The pressure is seen to switch to positive further back in the undisturbed case,
419 resulting in a more effective blade. For the 1D offset case, it displays the minor changes
420 in pressure along the surface of the blade, significantly towards the tip, at which point
421 the greatest amount of time is spent in the disturbed airflow of the wake.

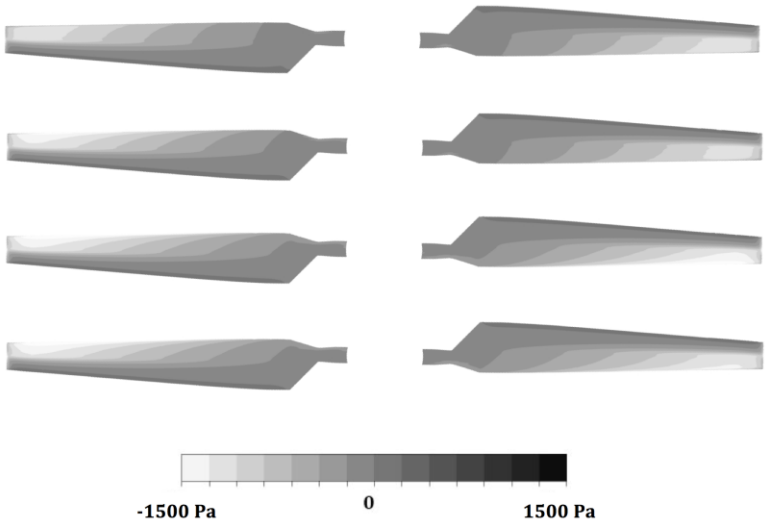

Figure 3.4 Pressure contour plots on the suction surface of the blades for cases: No upstream AD (first). Rotor 7D downstream: of aligned AD (second), 0.5D offset AD (third) - out of wake (left) and behind the wake (right), and 1D offset AD (fourth) - out of wake (left) and behind the wake (right).

The reason for using a full rotor simulation is that it allows for the calculation of torque along the blade as it rotates in and out of the incoming wake. Figure 3.5 illustrates the relative blade of interest as it completes a full rotation, the dotted line describes the approximate position of the incoming wake for the 0.5D offset case; the actual wake diameter will vary depending on the distance between turbines. The torque at r/R=0.7 along a single blade is plotted for a full rotation in Figure 3.6, and shows a periodic variation in the torque that the turbine experiences with a non-uniform flow upstream. As the blade enters the wake the torque falls rapidly, and in the case of 0.5D offset, it drops lower than the fully aligned layout. This is due to a combination of a lower wind velocity due to the wake and that low velocity changing the relative flow angle onto the rotor. At around 90˚ the blade is passing through the centre of the wake and so torque production is at its lowest, from this point it begins to rise again as the blade leaves the wake and into undisturbed air, where it eventually reaches a maximum point on the same level as the ideal, or no upstream turbine case.

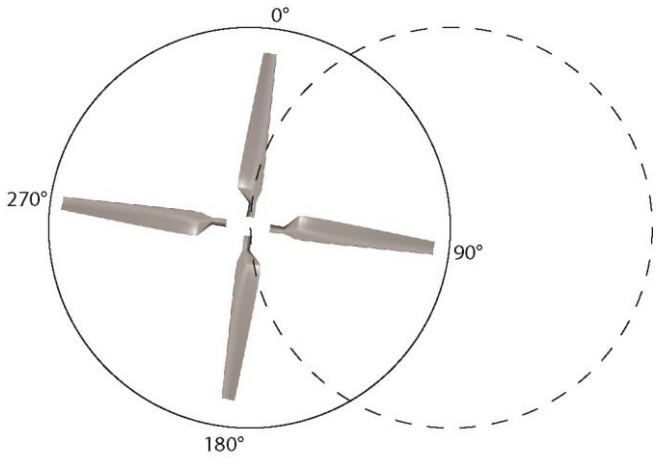

441

442 **Figure 3.5 Relative position of a single turbine blade relative to upstream wake for case 0.5D offset. The**
443 **actual wake width varies depending on distance between wind turbines.**

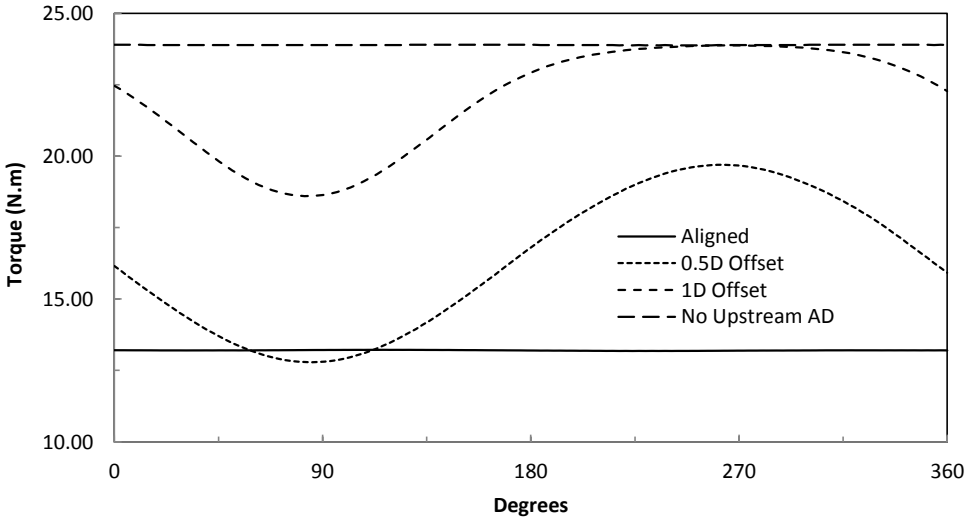

444

445 **Figure 3.6 Torque plot for position r/R=0.7 on a single blade throughout one rotation for case 7D.**

446 The wind turbines found in the second row of an array have been shown to
447 perform poorer when compared to those in the third row [20], [21]. The torque plot
448 shown in Figure 3.7 depicts the torque along a point on the blade through a single
449 rotation for both cases. It reflects that the torque production for a wind turbine in the
450 third row is significantly improved, especially for the cases for where there is increased
451 interaction with the wake from another rotor.

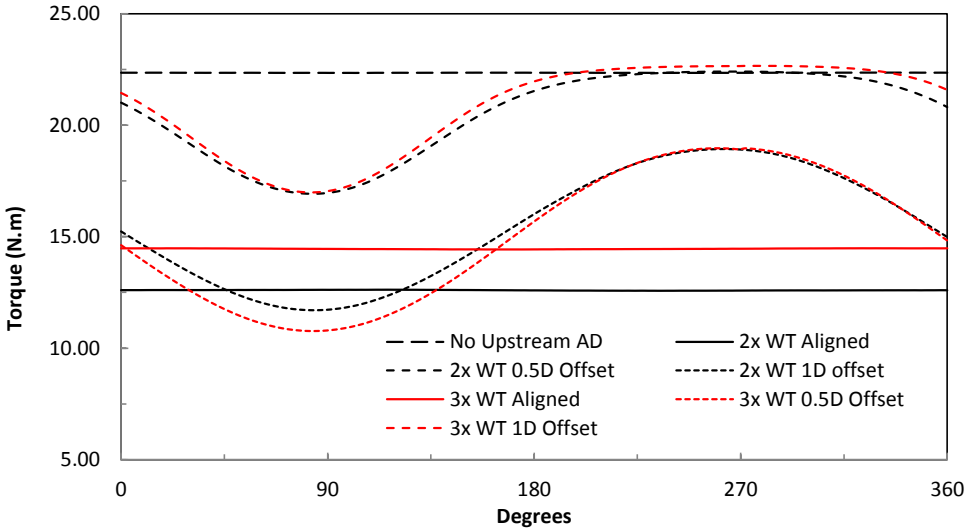

452

453 Figure 3.7 Torque plot for position r/R=0.7 on a single blade throughout one rotation comparing the second
454 and third turbine in row at 7D apart.

455 ## 4 Conclusion

456 The aim of this paper has been to develop and validate a technique that can be used
457 to determine the effects on performance that the wake from a wind turbine has on
458 downstream turbines. This was done by using actuator disc theory modelled using CFD
459 and combining this solution with a high fidelity CFD model of a full wind turbine rotor.
460 The advantage of this method is that it considerably reduces computational time and
461 cost, while still allowing detailed analysis of the performance and detailed
462 aerodynamics of a downstream turbine.

463 As a reference point, the modelled wind turbine CP was normalised to 1 when there
464 was no upstream wake present. However, this performance reduced drastically when
465 the introduction of a second wind turbine upstream (using the actuator disc model).
466 The maximum drop in performance occurred when two rotors (actually the actuator
467 disc and the downstream turbine) are aligned.

468 Analysis of static pressure along the blade showed that as a result of wake
469 interactions, a large reduction in the suction peak along the leading edge reduced the lift
470 generated by the rotor and so reduced the torque production and the ability for the
471 blade to extract energy from the wind.

Understanding the aerodynamics in these conditions can contribute to future designs for maximising energy yield within wind farms.

Acknowledgements

This research was funded and conducted as part of the WindNet research group at the University of Sheffield, UK. The authors would like to thank all those who have reviewed and contributed to this paper for their valuable assistance.

References

[1] D. Sturge, A. While, and R. Howell, "Engineering and energy yield: The missing dimension of wind turbine assessment," *Energy Policy*, vol. 65, pp. 245–250, Nov. 2014.

[2] J. Zoellner, P. Schweizer-Ries, and C. Wemheuer, "Public acceptance of renewable energies: Results from case studies in Germany," *Energy Policy*, vol. 36, pp. 4136–4141, Nov. 2008.

[3] R. Cowell, G. Bristow, and M. Munday, "Acceptance, acceptability and environmental justice: the role of community benefits in wind energy development," *J. Environ. Plan. Manag.*, vol. 54, no. 4, pp. 539–557, May 2011.

[4] DCLG, "National Planning Policy Framework," 2012.

[5] A. Betz, "Das Maximum der theoretisch moglichen Ausnutzung des Windes durch Windmotoren," *Zeitschrift für das gesamte Turbinenwes.*, no. 26, pp. 307–309, 1920.

[6] L. J. Vermeer, J. N. Sørensen, and A. Crespo, "Wind turbine wake aerodynamics," *Prog. Aerosp. Sci.*, vol. 39, pp. 467–510, Aug. 2003.

[7] B. Sanderse, "Aerodynamics of wind turbine wakes Literature review," Energy research Centre of the Netherlands, 2009.

[8] P. Réthoré, P. Van Der Laan, N. Troldborg, F. Zahle, and N. N. Sørensen, "Verification and validation of an actuator disc model," *Wind Energy*, 2013.

[9] G. España, S. Aubrun, S. Loyer, and P. Devinant, "Spatial study of the wake meandering using modelled wind turbines in a wind tunnel," *Wind Energy*, vol. 14, pp. 923–937, 2011.

[10] P. Weihing, K. Meister, C. Schulz, T. Lutz, and E. Krämer, "CFD Simulations on Interference Effects between Offshore Wind Turbines," *J. Phys. Conf. Ser.*, vol. 524, p. 012143, Jun. 2014.

[11] S. Ivanell, J. N. Sørensen, R. Mikkelsen, and D. Henningson, "Analysis of Numerically Generated Wake Structures," *Wind Energy*, vol. 12, pp. 63–80, 2009.

[12] J. Whale, C. . Anderson, R. Bareiss, and S. Wagner, "An experimental and numerical study of the vortex structure in the wake of a wind turbine," *J. Wind Eng. Ind. Aerodyn.*, vol. 84, no. 1, pp. 1–21, Jan. 2000.

[13] L. A. M. Danao, "The Influence of Unsteady Wind on the Performance and Aerodynamics of Vertical Axis Wind Turbines," The University of Sheffield, 2012.

505 [14] ANSYS, “ANSYS Fluent 12.0 User’s Guide,” 2009.

506 [15] D. Cabezón, J. Sanz, I. Marti, and A. Crespo, “CFD modelling of the interaction between the Surface
507 Boundary Layer and rotor wake. Comparison of results obtained with different turbulence models and
508 mesh strategies,” *Eur. Wind Energy Conf.*, 2009.

509 [16] B. Sanderse, S. P. van der Pijl, and B. Koren, “Review of computational fluid dynamics for wind turbine
510 wake aerodynamics,” *Wind Energy*, vol. 14, pp. 799–819, 2011.

511 [17] ANSYS, “ANSYS Fluent 12.0 Theory Guide,” 2009.

512 [18] D. Cabezón, E. Migoya, and A. Crespo, “Comparison of turbulence models for the computational fluid
513 dynamics simulation of wind turbine wakes in the atmospheric boundary layer,” *Wind Energy*, vol. 14,
514 pp. 909–921, 2011.

515 [19] M. M. Hand, D. A. Simms, L. J. Fingersh, D. W. Jager, J. R. Cotrell, S. Schreck, and S. M. Larwood,
516 “Unsteady Aerodynamics Experiment Phase VI: Wind Tunnel Test Configurations and Available Data
517 Campaigns,” 2001.

518 [20] R. J. A. M. Stevens, D. F. Gayme, and C. Meneveau, “Large eddy simulation studies of the effects of
519 alignment and wind farm length,” *J. Renew. Sustain. Energy*, vol. 6, no. 2, Mar. 2014.

520 [21] F. Porté-Agel, Y.-T. Wu, and C.-H. Chen, “A Numerical Study of the Effects of Wind Direction on
521 Turbine Wakes and Power Losses in a Large Wind Farm,” *Energies*, vol. 6, no. 10, pp. 5297–5313, Oct.
522 2013.

523 [22] J. Meyers and C. Meneveau, “Optimal turbine spacing in fully developed wind farm boundary layers,”
524 *Wind Energy*, vol. 15, pp. 305–317, 2012.

525